# Continuous Patient-Independent Estimation of Respiratory Rate and Blood Pressure Using Robust Spectro-Temporal Features Derived From Photoplethysmogram Only

Muhammad Ahmad Sultan and Wala Saadeh, *Senior Member, IEEE*

***Abstract*—*Objective:*** **A patient-independent approach for continuous estimation of vital signs using robust spectro-temporal features derived from only photoplethysmogram (PPG) signal.** ***Methods:*** **In the pre-processing stage, we remove baseline shifts and artifacts of the PPG signal using Incremental Merge Segmentation with adaptive thresholding. From the cleaned PPG, we extract multiple parameters independent of individual patient PPG morphology for both Respiration Rate (RR) and Blood Pressure (BP). In addition, we derived a set of novel spectral and statistical features strongly correlated to BP. We proposed robust correlation-based feature selection methods for accurate RR estimates. For fewer computations and accurate measurements of BP, the most significant features are selected using correlation and mutual information measures in the feature engineering part. Finally, RR and BP are estimated using breath counting and a neural network regression model, respectively.** ***Results:*** **The proposed approach outperforms the current state-of-the-art in both RR and BP. The RR algorithm results in mean absolute errors (median, 25th-75th percentiles) of 0.4 (0.1–0.7) for CapnoBase dataset and 0.5(0.3-2.8) for BIDMC dataset without discarding any data window. Similarly, BP approach has been validated on a large dataset derived from MIMIC-II (∼1700 records) which has errors (mean absolute, standard deviation) of 5.0(6.3) and 3.0(4.0) for systolic and diastolic BP, respectively. The results meet the American Association for the Advancement of Medical Instrumentation (AAMI) and British Hypertension Society (BHS) Class A criteria.** ***Conclusion:*** **By using robust features and feature selection methods, we alleviated patient dependency to have reliable estimates of vitals.**

***Index Terms*—Blood Pressure (BP), minimal redundancy maximal relevance (mRMR), photoplethysmogram (PPG), respiration rate (RR), signal quality, vitals, and wearable sensing.**

***Impact Statement*— Continuous, robust, and non-invasive monitoring of vitals with only one wearable sensor having applications in remote, fitness, and mobile healthcare devices where both RR and BP are desired.**

Manuscript received 31 July 2023; revised 20 September 2023 and 26 October 2023; accepted 26 October 2023. Date of publication 2 November 2023; date of current version 15 August 2024. This work was supported in part by Engineering and Design Department, Western Washington University (WWU) and in part by Islamic Development Bank (IsDB), Transform Fund. The review of this paper was arranged by Associate Editor Marianna Laviola. *(Corresponding author: Wala Saadeh.)*

Muhammad Ahmad Sultan is with the Electrical Engineering Department, Lahore University of Management Sciences (LUMS), Lahore 54792, Pakistan (e-mail: m_sultan@lums.edu.pk).

Wala Saadeh is with the The Engineering and Design Department, Western Washington University (WWU), Bellingham, WA 98225 USA (e-mail: saadehw@wwu.edu).

Digital Object Identifier 10.1109/OJEMB.2023.3329728

## I. Introduction

RESPIRATORY Rate (RR) and Blood Pressure (BP) are two vital health signs that help in timely diagnosis of various chronic respiratory and cardiovascular diseases (CVD) [1], [2]. Many health conditions such as sleep apnea, asthma, and hypertension require monitoring both RR and BP [3], [4], [5]. Obstructive sleep apnea (OSA) is a sleep disorder due to breathing problems, characterized by partial or full occlusion of the upper airway during sleep which can generate sleep fragmentation and recurrent oxyhemoglobin desaturations [6]. Sleep RR is a key sign of critical illness, particularly for OSA monitoring. RR of healthy adults in a relaxed state is around 12–20 breaths/minute (bpm). However, the RR will be abnormal for the OSA case when the sleep breathing is decreased or halted by the apnea [7]. Therefore, sleep RR is a primary and key indicator for OSA patients. OSA which is considered a major risk factor for CVD degrades human health and occasionally leads to nocturnal death [8]. BP is part of the assessment of cardiovascular risk. In patients with OSA, CVDs have a higher incidence and are linked to worse functional results and higher mortality rates. Systemic hypertension, which is usually present in OSA, can significantly degrade cardiovascular health. In addition, fluctuating BP may induce a further risk of higher incidence and rapid progression of CVD. Therefore, for OSA patients it is essential to monitor both BP and RR at the same time. Continuous monitoring of RR and BP using wearable sensors can predict CVD earlier for timely treatment and thus, can prevent severe conditions leading to death [9].

Traditionally, measurement of vital signs requires wearing bulky uncomfortable sensors which are performed in a hospital with cumbersome devices. Respiration is observed using capnometry or spirometry in clinical settings. Similarly, BP is measured conventionally using a cuff-based method with a mercury

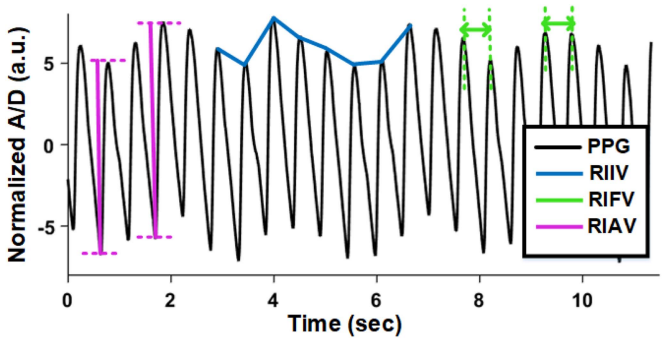


**Fig. 1.** PPG signal with arbitrary units (a.u.) showing the respiratory Induced Variations (RIVs), where RIIV is the variation in beat peaks (Envelope). RIFV is the changes in the inter-beat interval. RIAV is the change in the beat strength.

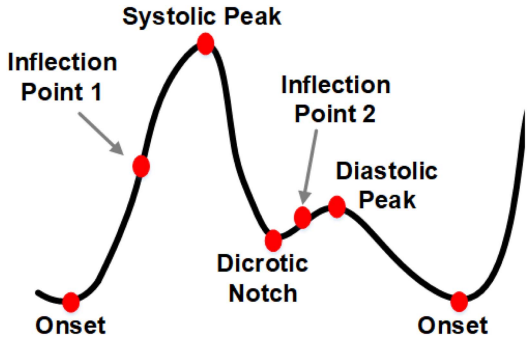


**Fig. 2.** Ideal PPG Morphology exhibiting morphological features for Blood Pressure Estimation.

sphygmomanometer [9]. The cuff makes this method inconvenient for frequent usage. These traditional methods prevent continuous monitoring of vitals which is required for accurate diagnosis and treatment of CVD in a timely manner.

Recent research focuses on continuous monitoring of vital signs using convenient wearable Photoplethysmogram (PPG) sensors [10], [11], [12], [13], [14]. [15] utilizes a multi-layer convolutional encoder–decoder framework that takes PPG as an input and outputs respiratory waveforms. An end-to-end pipeline for RR estimation using Cycle Generative Adversarial Networks (CycleGAN) to reconstruct respiratory signals from raw PPG signals was presented in [14] while an end-to-end deep learning model which does not require feature engineering with raw PPG signals as input was described in [16]. An automated Hilbert envelope-based respiration rate estimation method using the PPG signal was proposed in [17]. RR can be also measured by deriving respiration trends from the PPG signal as explained comprehensively in our previous work [18]. Respiration modulates PPG in three ways: 1) Respiratory-induced intensity variation (RIIV), 2) Respiratory-induced frequency variation (RIFV), and 3) Respiratory-induced amplitude variation (RIAV) [16], [19]. Fig. 1 elaborates these three induced variations from PPG for respiration. Nevertheless, the existence of these modulations relies on several factors such as gender, age, patient's health, and body position during measurement. They may also appear and disappear for certain patients over time. The traditional fusion approach for RR estimation provides equal weight (finds the mean) to RR estimates from the overall modulations without observing the respiration quality of the individual modulation waveforms. This method raises the mean absolute error (MAE) remarkably for many patients, degrading the overall measurement accuracy. The smart fusion method enhances robustness, however, it disregards several data windows which decreases the system throughput. The technique in [19] utilizes an automatic algorithm that selects the modulation segment with the highest respiratory quality indices (RQIs) for RR estimation. Secondly, the Kalman smoother (KS) is used to fusion multiple modulations with RQI above a given threshold. However, it needs an Electrocardiogram (ECG) signal in addition to PPG as inputs. In this paper, we propose a Modulation Quality Index (MQI) based fusion approach that mitigates the challenge of patient dependency, offering robust and continuous RR measurements. We incorporated more vigorous MQIs and we consider the mean of only those RR readings which were computed from exceptional standard and trustworthy modulation patterns. The proposed method enhances the RR measurements by decreasing the MAE by >20% compared to [16], [19].

For cuffless continuous BP monitoring, Pulse Wave Velocity (PWV) methods have shown a great impact [20], [21]. Recent PWV-based approaches use Pulse Arrival Time (PAT) and Pulse Transit Time (PTT) which describe cardiovascular characteristics in terms of blood vessels' expansion and contraction. These parameters are extracted from two physiological signals i.e., PPG and Electrocardiogram (ECG) signals [22], [23], [24]. The acquisition of two physiological signals, however, makes the implemented device more complex. These approaches not only increase hardware complexity but also add to the patient's discomfort by wearing and carrying multiple sensors for continuous use. To determine blood pressure from PPG only, there is no straightforward mathematical relation between PPG and BP. However, variation in PPG morphology appears to be correlated to BP [24], [25], [26], [27]. Therefore, an artificial intelligence tool is required to uncover the hidden relation. In the literature, deep learning was involved where features are automatically extracted from time-domain signal and spectrum using fully connected and convolutional layers [24], [28], [29]. Deep learning methods have also been proposed recently using visibility graphs (VG). The work in [27] presented a data-driven deep-learning-based end-to-end solution for estimating BP from the short-duration PPG signals using VG and pre-trained deep convolutional neural network (CNN) for image classification. Hybrid neural network architecture consists of convolutional, recurrent, and fully connected layers that operate directly on the raw PPG time series and provide BP estimation has been presented in [28]. However, machine learning methods based on handcrafted features are more reliable when there exist physical relations between features and the target variable [24], [26]. Previous studies have relied heavily on the PPG morphology to derive various parameters such as diastolic peaks, inflection points, and dicrotic notch [26], as shown in Fig. 2. The study in [26] has used only the PPG signal but it depends on

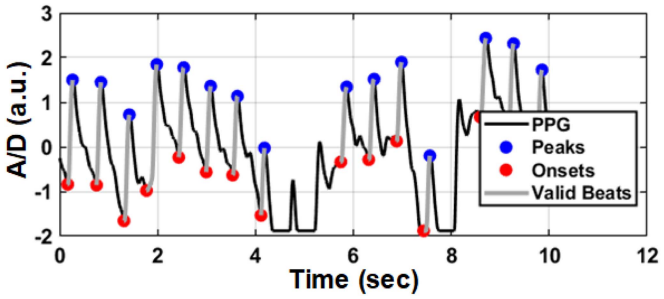


**Fig. 3.** Output of IMS Algorithm showing peaks and onsets of valid beats. The remaining beats are artifactual having clipped or saturated pulses.

accurate and reliable extraction of these morphological features and they have validated their approach on a small dataset (only 21 patients). It has been noted that these methods do not work when the feature extraction process gets erroneous due to variation of the PPG morphology from patient-to-patient. Few studies have explored the spectral features but they cannot work solely; they need morphological parameters to estimate BP as well [22], [23]. Therefore, both spectral and statistical features that are morphology-independent are essential to obtain robust BP readings.

In this study, we propose a single-channel PPG with a patient-independent approach for BP estimation. We utilize a few morphological parameters such as peak and onset which are present in every PPG morphology as well as robust frequency domain features based on spectral energy, entropy, and area. The presented technique outperforms the current state-of-the-art ([22], [26], [27]) while being validated on a larger and more diverse database. Our dataset has almost double the number of patient cases (approx. 1700 patients) compared to [26], [27], and [28], which proves the clinical robustness of our proposed approach.

The proposed methodology involves a common pre-processing step for both RR and BP estimations which includes baseline wandering and artifact removal caused by body motion. However, BP and RR differ in extracted features and estimation methods afterward and hence are explained in separate sections. This paper is organized as follows: Section II-A introduces pre-processing step of PPG filtering and segmentation. Sections II-B and II-C present feature extraction and feature selection for both RR and BP. Section II-D describes RR and BP estimation methods. In Section III, the results are described. The discussion and conclusion are detailed in Sections IV and V, respectively.

## II. Materials and Methods

The proposed methodology is presented in the block diagram Fig. 4. A) The patient's PPG signal obtained using a pulse oximeter goes to preprocessing block where it is filtered, and artifacts are identified. B) Physiological features i.e., RIIV, RIFV, and RIAV are extracted for characterizing respiration activity. For Blood Pressure estimation, we extract different physiological, spectral, and statistical features. C) Extracted features are then analyzed for their significance in estimating RR and BP using feature selection methods. Selected features then go to the final estimation block. D) RR is computed using the breath counting method and an average measurement is generated over the selected modulation RRs for the desired PPG window. Similarly, BP is estimated using a Deep Neural Network (DNN) regression model. Finally, at the output terminal, we have desired values of RR, systolic BP, and diastolic BP.

### A. Pre-Processing

First, we filter the PPG signal using a bandpass filter (0.05–10 Hz) to remove both low and high-frequency noise. Then, baseline shifts are removed to observe main respiration and cardiac activities. This is achieved by removing the varying dc value from the PPG signal over time. PPG beats and artifacts are characterized through Incremental Merge Segmentation (IMS) and adaptive thresholding [30]. The IMS algorithm utilizes a sliding-window technique which is straightforward, rapid, and can be measured in run-time. In this segmentation algorithm, line segments are formed using their slopes first. Then up-slope segments are classified as valid beats and artifacts based on their amplitude and inter-beat interval thresholds. This method deploys adaptive thresholding which adapts to the PPG morphology and results in the accurate detection of PPG key points for robust discrimination of valid beats and artifacts. It detects artifacts of both types i.e., motion artifacts having abnormal amplitude and clipping noise having flat horizontal lines due to sensor disconnection. Within each processing window, we use only valid beats for the detection of key points to accurately extract features from it.

From the IMS algorithm, we detect peaks and onsets of valid beats along with motion and clipping artifacts (Fig. 3). The time series of PPG is defined as $\{t_i,\, x_i\}_{i=1\ldots N}$ where $N$ is the length of the PPG signal. Then we can define the time series of detected peaks as $\{t_{peak,i},\, x_{peak,i}\}_{i=1\ldots N_{peak}}$ and time series of detected onsets as $\{t_{onset,i},\, x_{onset,i}\}_{i=1\ldots N_{onset}}$ where $N_{peak}$ and $N_{onset}$ are the number of peaks and number of onsets, respectively, and $N_{peak} = N_{onset} =$ Number of valid beats identified. The detected key points of valid PPG beat i.e., peaks and onsets are used to extract temporal features for both RR and BP estimations, as discussed in the next section in detail.

### B. Feature Extraction

After filtering the signal for artifacts, we extract useful features from valid PPG beats to measure RR and BP. These features depend on powerful time-domain and frequency-domain parameters that lead to robust estimation of RR and BP. Note that our proposed system requires only one physiological signal i.e., PPG while approaches described in [22], [23], [24], [25] need two signals i.e., ECG and PPG to extract PTT and PAT-related features. However, we have reduced system complexity by using only the PPG signal as input. For RR and BP estimation, we extract three sets of features from PPG only. These consist of PPG morphology, spectrum, and statistical parameters, as discussed below in detail:

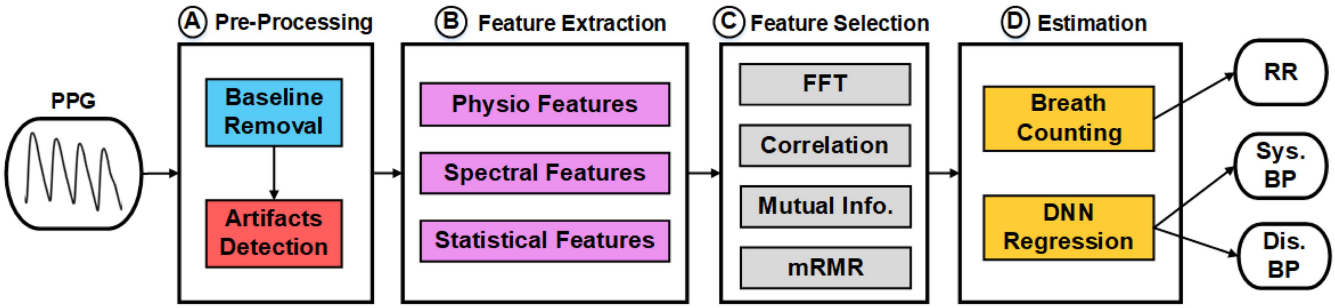


**Fig. 4.** Proposed approach. A: Baseline shifts of raw PPG are removed, and artifacts are identified. B: Physio, spectral and statistical features are extracted from cleaned PPG. C: Extracted features are checked for their relative significance in determining RR and BP. D: Finally, RR is estimated using breath counting, and BP (Systolic and Diastolic) is measured using a DNN regression model.

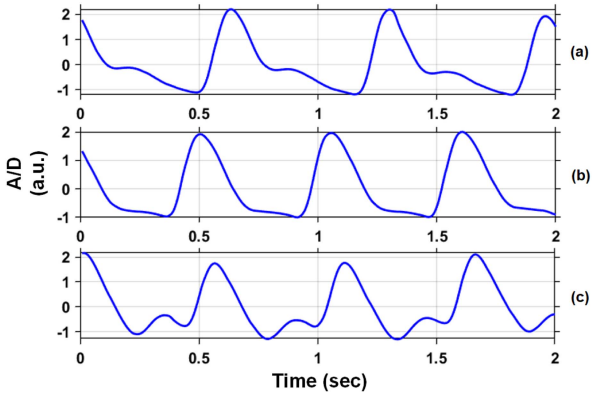


**Fig. 5.** Three PPG signals with different morphologies from the MIMIC Database with (a) ideal morphology with visible critical points such as inflection point, dicrotic notch, and systolic and diastolic peaks, (b) and (c) nonideal shapes of PPG morphology due to missing or altered peaks/points such as inflection points, dicrotic notch, and diastolic peak.

***1) Morphological Features:*** These features depend on the morphology of the PPG waveform. Extraction of features involves determining key points of the PPG signal. Here we have used only peaks and onsets of PPG detected in preprocessing stage because other key points (diastolic peak, dicrotic notch, and inflection points) are highly dependent on PPG morphology which varies from patient to patient as the cardiovascular characteristics and skin textures vary. Extraction of other key points leads to the erroneous calculation of features [18]. Fig. 5 shows three different PPG morphologies obtained from different subjects. All three PPG signals are free from artifacts or noise. First PPG has ideal morphology which presents critical points such as inflection point, dicrotic notch, and diastolic peak along with systolic peak and onset. However, the last two PPGs have altogether different morphology although they are correct. This difference in morphology leads to incorrect calculation of morphological parameters which decreases the reliability of the system. Therefore, we have limited morphological parameters' extraction to peaks and onsets only. We have focused more on spectral and statistical features whose calculation is accurate. In this way, we have alleviated the problem of patient morphology variation and developed a patient-independent approach. Here we extract three respiratory modulations for RR estimation and five morphological parameters for BP estimation.

As discussed earlier, three respiratory variations can be derived from PPG: 1) PPG peaks changes during respiration, forming RIIV. 2) Inter-beat interval changes i.e., compressed beats during inhalation and expanded beats during exhalation i.e., RIFV. 3) Amplitude of up-slopes of beats variations, forming RIAV. From the peaks and onsets determined in preprocessing stage, we obtain the following three respiratory modulations for RR estimation:

1) *RIIV:* This is time series of amplitudes of PPG peaks i.e., $x_{RIIV} = \{t_i, x_{peak,i}\}_{i=1...N_{peak}}$. This effect represents intrathoracic pressure variations, resulting in the change of perfusion baseline.
2) *RIFV:* It is the time between successive PPG peaks; $x_{RIFV} = \{t_i, x_{RIFV,i}\}_{i=1...(N_{peak}-1)}$ where $x_{RIFV,i} = t_{j+1} - t_j$ for $t_j$ the time series of peaks. This phenomenon is known as Respiratory Sinus Arrhythmia (RSA) which is regulated by the vagal nerve.
3) *RIAV:* Amplitude difference between the peak and onset of a beat; $x_{RIAV} = \{t_i, x_{RIAV,i}\}_{i=1...N_{peak}}$, with $x_{RIAV,i} = x_{peak,i} - x_{onset,i}$. This effect is caused by cardiac output variations which represent refill quantity in the vessels at the periphery.

Fig. 6 shows a 32-sec window of PPG signal with detected beats (onsets and peaks). From the identified peaks and onsets, we derive three modulations i.e., RIIV, RIFV, and RIAV. These derived modulations are re-sampled to 4 Hz with linear interpolation. Next, we calculate morphological parameters for BP estimation (Fig. 7). These features represent peripheral resistance and arterial stiffness in terms of pulse expansion and contraction in the systolic and diastolic regions of PPG.

1) *Systolic Time:* It is the time between beat start (onset) and beat peak. It represents upstroke beat expansion. This parameter is related to the stiffness of blood arteries. Mathematically, $t_{sys,i} = t_{peak,i} - t_{onset,i}$.
2) *Diastolic Time:* It is the time between beat peak and beat end (onset of next beat); $t_{dias,i} = t_{onset,i+1} - t_{peak,i}$.
3) *Systolic and Diastolic Branch widths:* It is the systolic or diastolic time calculated at a fraction of beat amplitude: $t_{X,sys,i} = t_{peak,i} - t_{X,i}$ where $t_{X,i} : x_i = X * x_{peak,i}$ and X = [0.1, 0.25, 0.33 0.5]. For example, $t_{33,sys}$ is the

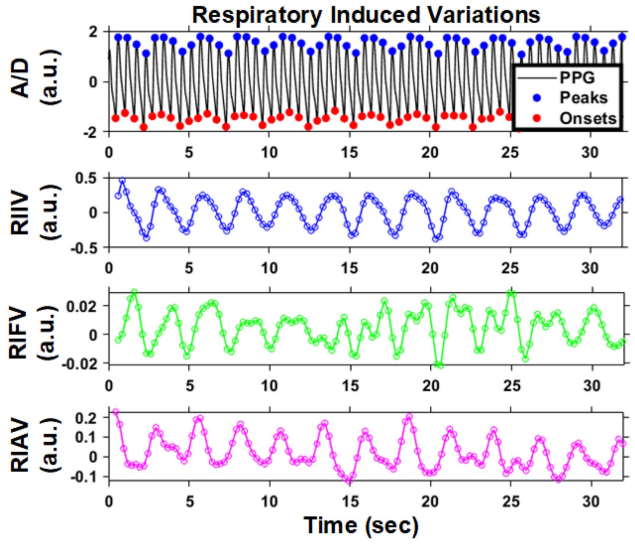


**Fig. 6.** 32 sec PPG window displaying Physiological Feature Extraction for RR estimation: RIIV, RIFV, and RIAV are formed using identified peaks and onsets, and then re-sampled to 4 Hz. RIIV is the most accurate representation of respiration activity.

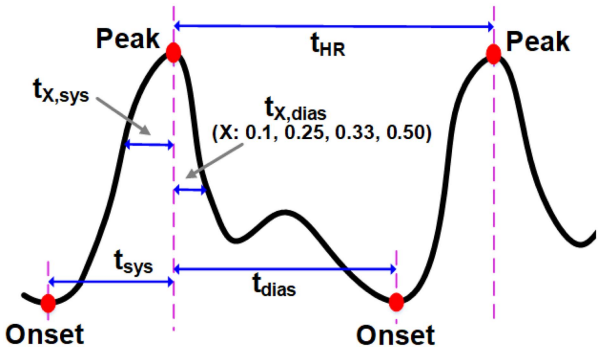


**Fig. 7.** Morphological features extracted from PPG morphology for BP estimation.

time when beat amplitude is 33% of the beat peak. This is also a way of characterizing PPG morphology using pulse expansion. Similarly, we can calculate different percentages of diastolic time. These branch widths at different percentages of amplitude are related to total peripheral resistance.

4) *Heart Rate:* It is the time between two consecutive beats, representing one cardiac cycle; $t_{HR,i} = t_{peak,i+1} - t_{peak,i}$.
5) *PPG Intensity Ratio:* It is the ratio of peak and onset amplitudes. It shows the amplitude intensity of the pulse. We take the average of all valid beats' peaks and onsets during the given window for accurate calculation. $PIR_i = x_{peak,i}/x_{onset,i}$.

These features are calculated for only those PPG beats which have been detected as valid beats by the IMS algorithm in the pre-processing stage. We extract per-cycle parameters such as systolic and diastolic times from individual cycles, and then we average them over the current processing window. Note that these morphological features are valid for all PPG morphologies

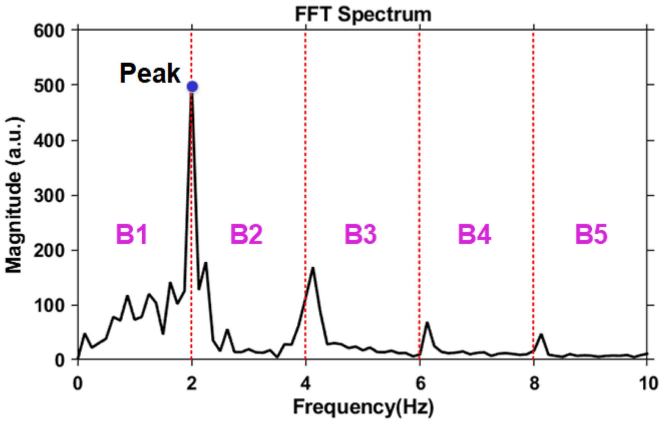


**Fig. 8.** PPG Spectrum showing 5 frequency bands from 0 to 10 Hz for Spectral Feature Extraction.

presented in Fig. 5. Next, we extract the spectral and statistical features which are calculated for only those PPG windows that have artifacts less than an empirical threshold.

***2) Spectral Features:*** Here we take FFT to get the power spectrum of the PPG signal represented as $H(w)$, for frequency-domain feature extraction (Fig. 8). The spectrum frequencies are concentrated in the range of 0 to 10 Hz, which is the plausible range for PPG. We first take the spectrum peak and the corresponding frequency (which is the heart rate) as features. Then we divide the 10 Hz spectrum into 5 equal parts i.e. [0–2, 2–4, 4–6, 6–8, 8–10]. We selected 5 as the number of bands empirically after observing the main frequency content variation in these regions of the FFT spectrum. Then we calculate the following features from these bands as follows:

1) *Energy bands:* Energy in different frequency bands shows the frequency content in a particular band. We calculate normalized spectral energy for each frequency band, given as:

$$Energy = \frac{1}{N}\sum_{i=1}^{N} |H(w_i)|^2, \tag{1}$$

where N is the number of frequency components in a particular band. The extracted spectral energies relate to the frequency content of the PPG signal which varies with BP.
2) *Entropy bands:* Entropy gives the amount of information present in a particular band. We calculate spectral entropy for each frequency band using normalized frequency components $H(w_i)_N$;

$$\text{Entropy} = -\sum_{i=1}^{N} H(w_i)_N \cdot \log\left(H(w_i)_N\right), \tag{2}$$

where $H(w_i)_N = H(w_i)/\sum_{i=1}^{N} H(w_i)$
3) *Area bands:* The area under the spectrum for each frequency band has been calculated using the trapezoidal

method:

$$\text{Area} = \frac{1}{2}\sum_{i=1}^{N-1}\left[H\left(w_i\right) + H\left(w_{i+1}\right)\right].\left(w_{i+1} - w_i\right), \tag{3}$$

These parameters signify the harmonic content of the PPG signal which is related to cardiac and respiratory activities. These frequency-domain features are highly correlated to the output BP values which makes our method robust (discussed below).

***3) Statistical Features:*** We extracted a set of temporal features based on statistics as well. These features model PPG physiology variations in statistical ways. These include time-domain PPG signal's kurtosis, skewness, and temporal entropy as important statistical parameters:

1) *Kurtosis:* It shows the flatness of a signal which is a statistical way of describing the signal shape.

$$\text{Kurtosis} = \frac{\sum_{\text{i=1}}^{\text{N}}\left(\text{x}_\text{i} - \bar{\text{x}}\right)^4}{\text{N}.\left(\sqrt{\text{c}}\right)^4} \tag{4}$$

where $N, \bar{x}, c$ are signal length, signal mean, and variance, respectively in the current processing window.

2) *Skewness:* This parameter checks symmetry of signal distribution.

$$\text{Skewness} = \frac{\sum_{\text{i=1}}^{\text{N}}\left(\text{x}_\text{i} - \bar{\text{x}}\right)^3}{\text{N}.\left(\sqrt{\text{c}}\right)^3}, \tag{5}$$

3) *Temporal Entropy:* This is the information entropy of the PPG signal, calculated from the probability distribution of the normalized signal.

$$\text{Entropy} = -\sum_{\text{i=1}}^{\text{N}} \text{x}_{\text{n,i}} \cdot \log\left(\text{x}_{\text{n,i}}\right), \tag{6}$$

where $x_{n,i} = x_i / \sum_{i=1}^{N} x_i$

As described earlier, PPG morphology varies from patient to patient subject to cardiovascular properties and skin texture. Similarly, the prominence of morphological features i.e., RIIV, RIFV, and RIAV for RR estimation also vary due to several factors including age, health condition, and activity during measurement. Among the extracted modulations (Fig. 6), RIIV is the most realistic depiction of the respiration pattern whereas both the RIFV and RIAV are absent in the displayed PPG graph. Therefore, we need to check the quality of extracted modulation before estimating RR from it. Similarly, A total of 35 features were extracted for BP estimation including morphological, spectral, and statistical features (Table I). However, using all the features increases computational load and regression model complexity. Therefore, we performed feature relevance and redundancy analysis and selected only the top 12 features which are most relevant to the target BP value and least redundant within the selected feature set.

**TABLE I**
LIST OF FEATURES EXTRACTED FOR BP ESTIMATION

| Index | Feature | Definition |
|---|---|---|
| 1. | t_sys | Systolic upstroke time between beat start and peak |
| 2. | t_dias | Diastolic time between beat peak and beat onset |
| 3. | t_10,sys | |
| 4. | t_25,sys | Systolic time at X% of beat amplitude |
| 5. | t_33,sys | (X: 10, 25, 33, 50) |
| 6. | t_50,sys | |
| 7. | t_10,dias | |
| 8. | t_25,dias | Diastolic time at X% of beat amplitude |
| 9. | t_33,dias | (X: 10, 25, 33, 50) |
| 10. | t_50,dias | |
| 11. | t_HR | Heart Rate representing one cardiac cycle |
| 12. | PIR | PPG Intensity Ratio |
| 13. | PSD_peak | Power Spectrum peak amplitude |
| 14. | Energy_B1 | |
| 15. | Energy_B2 | Energy of frequency bands |
| 16. | Energy_B3 | (B1: 0-2, B2: 2-4, B3: 4-6, |
| 17. | Energy_B4 | B4: 6-8, B5: 8-10) Hz |
| 18. | Energy_B5 | |
| 19. | Entropy_B1 | |
| 20. | Entropy_B2 | Entropy of frequency bands |
| 21. | Entropy_B3 | (B1: 0-2, B2: 2-4, B3: 4-6, |
| 22. | Entropy_B4 | B4: 6-8, B5: 8-10) Hz |
| 23. | Entropy_B5 | |
| 24. | Area_B1 | |
| 25. | Area_B2 | Area of frequency bands |
| 26. | Area_B3 | (B1: 0-2, B2: 2-4, B3: 4-6, |
| 27. | Area_B4 | B4: 6-8, B5: 8-10) Hz |
| 28. | Area_B5 | |
| 29. | Perc_20 | |
| 30. | Perc_40 | $i^{th}$ percentile of temporal PPG |
| 31. | Perc_60 | (i: 20, 40, 60, 80) |
| 32. | Perc_80 | |
| 33. | Kurtosis | Statistical measure of PPG flatness |
| 34. | Skewness | Statistical measure of PPG Distribution Symmetry |
| 35. | Entropy | Information entropy of PPG |

## C. Feature Selection

Since the quality of extracted modulations for RR estimation depends heavily on patient health condition and activity, we require accurate quality assessment measures to estimate RR from extracted modulations. In the literature, PPG signal quality has been assessed in the pre-processing stage to detect artifacts. However, a little focus has been put into developing quality assessment measures for respiratory-induced variations [31], [32]. Here we present robust modulation quality indices (MQIs) based on Fourier analysis and correlation for RR:

1) *Power Spectrum MQI (FFT):* Fourier Analysis is utilized to study the frequency content of a signal. We measure the peak dominance of the FFT power spectrum to realize how strong the respiration frequency is compared to other frequencies in the extracted modulation.

$$MQI_{FFT} = P_{peak}/P_{total}, \tag{7}$$

where $P_{peak}$ is the summation of three power values centered on peak value and $P_{total}$ is the total power values in the plausible respiration range of 0.1 to 1 Hz (6 to 60 bpm). $MQI_{FFT}$ close to one means the spectrum peak is dominant over the whole spectrum, which means that the respiration frequency is strongly present in the modulation (Fig. 9).

2) *Autocorrelation MQI (AC):* Autocorrelation is utilized to study the signal periodicity. We find the modulation periodicity with a lag range from 1 to 10 seconds (k = 4 to 40 samples) corresponding to a plausible respiration

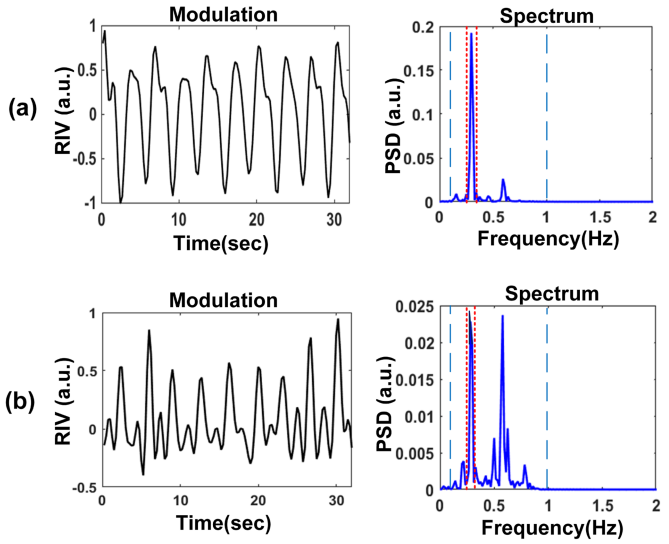


**Fig. 9.** Examples of two 32 sec extracted modulation window (left) and modulation power spectrum (right) where (a) shows that the respiration frequency is strongly present in the modulation, and (b) shows that the respiration frequency is weakly present in the modulation. The dotted blue margins indicate a plausible respiration range of 0.1 to 1 Hz (6 to 60 bpm) while red ones show 3 power frequency components middling the peak power value.

range of 6 to 60 bpm.

$$MQI_{AC} = \max\left\{\frac{\frac{1}{N-1}\sum_{i=1}^{N-k}(x_i-\bar{x})(x_{i+k}-\bar{x})}{c_0}\right\} \quad (8)$$

where $N, k, \bar{x}, c_0$ are signal length, time lag, signal mean, and variance, respectively. Closer the $MQI_{AC}$ is to 1, the more periodic modulation is.

3) *Template Matching MQI (XC-Tmp):* Cross-correlation is used to study the similarity between signals. We compared the similarity of the modulation with its smoothened version generated after passing a moving average filter considering a plausible respiration range of 0.1 to 1 Hz (6 to 60 bpm), known as template-matching.

$$MQI_{XC-Tmp} = \frac{\frac{1}{N-1}\sum_{i=1}^{N}(x_i-\bar{x})(y_i-\bar{y})}{\sqrt{c_x.c_y}}, \quad (9)$$

where $N, \bar{x}, \bar{y}, c_x, c_y$ are signal length, signal mean, template mean, signal variance, and template variance, respectively. The closer the $MQI_{XC-Tmp}$ is to 1, the more similar modulation is to its standard template (Fig. 10). Note that $MQI_{XC-Tmp}$ is computed only if the corresponding PPG window has percentage artifacts less than an empirical threshold. Other MQIs need not to check artifacts because they automatically identify artifactual portions in derived modulations. However, $MQI_{XC-Tmp}$ requires constructing a template out of the given modulation. Hence, the PPG window under analysis must be free from any artifacts.

Fig. 11 elaborates the effect of changing threshold values of one quality measure i.e., MQI-FFT on patient-wise performance (a) and data retention (b) for CapnoBase dataset. As we increase

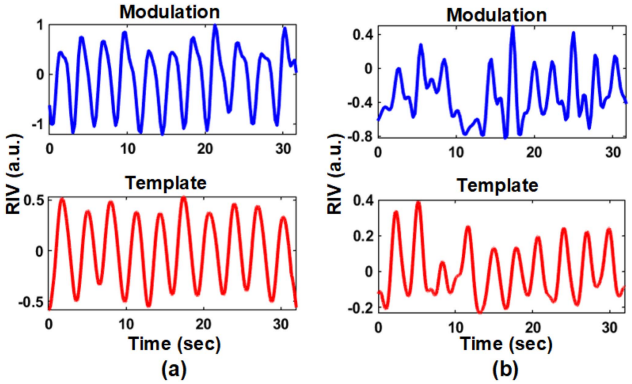


**Fig. 10.** Examples 32 sec window of extracted modulation (top) and templates (bottom) where (a) represents a good quality waveform having a strong correlation with the template, and (b) represents bad quality modulation having less $MQI_{XC-Tmp}$.

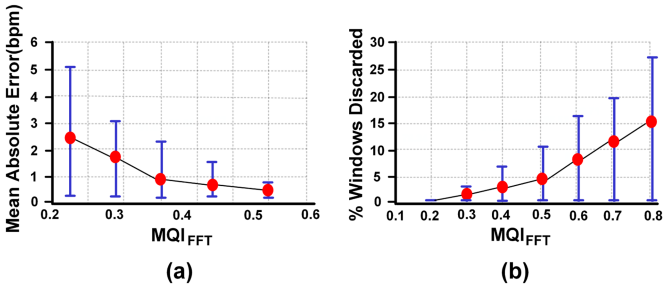


**Fig. 11.** Effect of changing Thresholds on (a) Performance measured through mean absolute error (bpm) and (b) DataRetention measured through % of windows discarded. As the threshold value is increased (strict quality thresholds), Error decreases at the expense of discarding many data windows. The red circle indicates the median and blue line boundaries denote the Inter-Quartile Range (25th to 75th percentiles).

the threshold values for lesser errors, we drop a lot of data windows. However, we tune the thresholds in such a way that we get optimal performance while retaining all the windows. Note that these threshold values are independent of a particular patient i.e., they are fixed for the whole dataset. Then the quality of each modulation is estimated using all the three MQIs illustrated earlier and only the high-quality modulations are adopted for the estimation of RR, which is vetted by all three metrics.

Feature relevance analysis reveals the significance of a particular feature for the target estimation and Feature redundancy analysis removes redundant features, lowering computational load and ML model complexity later.

1) *Pearson Correlation Coefficient:* To see the linear relationship of extracted features with target BP values, we use the Pearson correlation coefficient. It is calculated as:

$$PCC = \frac{\sum_{i=1}^{N}(x_i-\bar{x})(y_i-\bar{y})}{\sqrt{c_x.c_y}}, \quad (10)$$

where $N, \bar{x}, \bar{y}, c_x, c_y$ are feature-length, feature mean, target mean, feature variance, and target variance, respectively. The closer the PCC is to 1, the greater the linear dependency between the feature and target is.

2) *Mutual Information Coefficient:* Mutual information is used to find non-linear dependency between features

**TABLE II**
FEATURE SIGNIFICANCE SCORE OF TOP 18 RANKED FEATURES USING FOUR SELECTION MEASURES: PEARSON CORRELATION COEFFICIENT (PCC), MUTUAL INFORMATION COEFFICIENT (MIC), CORRELATION BASED MRMR (MRMR_PCC) AND MUTUAL INFORMATION BASED MRMR (MRMR_MIC)

| Feature | Feature Importance Score (scaled 0 to 1) | | | | |
|---|---|---|---|---|---|
| | PCC | MIC | mRMR (PCC) | mRMR (MIC) | Avg. Score |
| t_10,dias | 0.58 | 0.78 | 0.17 | 0.17 | 0.43 |
| **t_33,dias** | 0.63 | 0.96 | 0.63 | 0.96 | **0.80** |
| **t_25,dias** | 0.63 | 1.00 | 0.63 | 0.20 | **0.60** |
| **Energy_B1** | 0.74 | 0.81 | 0.74 | 0.43 | **0.68** |
| **Energy_B2** | 0.74 | 0.80 | 0.43 | 0.48 | **0.61** |
| **Kurtosis** | 0.76 | 0.58 | 0.97 | 0.97 | **0.82** |
| **t_25,sys** | 0.86 | 0.97 | 0.86 | 0.97 | **0.92** |
| **t_50,dias** | 0.87 | 0.79 | 0.26 | 0.79 | **0.68** |
| **t_33,sys** | 0.97 | 0.97 | 0.11 | 0.97 | **0.76** |
| **t_50,sys** | 1.00 | 0.88 | 0.14 | 0.88 | **0.73** |
| **Perc_60** | 0.22 | 0.80 | 0.89 | 0.89 | **0.70** |
| **t_10,sys** | 0.52 | 0.98 | 0.52 | 0.98 | **0.75** |
| **Entropy** | 0.49 | 0.41 | 1.00 | 1.00 | **0.73** |
| Entropy_B3 | 0.33 | 0.18 | 0.60 | 0.60 | 0.43 |
| Area_B2 | 0.54 | 0.28 | 0.71 | 0.28 | 0.45 |
| Energy_B5 | 0.01 | 0.25 | 0.01 | 0.51 | 0.20 |
| t_dias | 0.39 | 0.62 | 0.39 | 0.03 | 0.36 |
| Energy_B3 | 0.49 | 0.58 | 0.49 | 0.58 | 0.54 |

The bold face represents features with high average score.

and target variables. It is based on entropy measurement which reveals probabilistic relations among variables of interest. Entropy calculation involves probability distribution estimation by making histogram bins first. The mutual information Coefficient is given as:

$$MIC = \frac{I(X;Y)}{\sqrt{H(X).H(Y)}}, \tag{11}$$

Where $I(X;Y), H(X), H(Y)$ are mutual information between feature and target, the entropy of feature and entropy of target, respectively. MIC value close to 1 indicates strong mutual dependence between feature and target variables, which is highly desirable for decision trees deploying information gain as attribute selection criteria.

3) *Minimal Redundancy and Maximal Relevance (mRMR):* To verify that features selected by PCC and MIC are not redundant within themselves, we used this minimum redundancy analysis [33].

$$\max \left[ I\left(x_j; y\right) - \frac{1}{m-1} \sum_{x_i \in F_{m-1}} I\left(x_j; x_i\right) \right] \tag{12}$$

where $x_j \in X - F_{m-1}$, $I(x_j; y)$ is the MI between feature $x_j$ and target BP value y, and $I(x_j; x_i)$is the MI between features. Here X represents the complete feature vector while F denotes the selected feature set. This method selects features based on their maximum relevance to the target variable and their minimum redundancy among selected features. Note that we used this method for correlation-based dependency as presented in Table II.

**TABLE III**
PERFORMANCE COMPARISON OF IMPLEMENTED ML ALGORITHMS IN TERMS OF MEAN ABSOLUTE ERROR (MAE) AND STANDARD DEVIATION OF ERROR (SDE) FOR SBP, DBP, PP AND MAP

| ML Algorithm | SBP (mmHg) | | DBP (mmHg) | | PP (mmHg) | | MAP (mmHg) | |
|---|---|---|---|---|---|---|---|---|
| | MAE | SDE | MAE | SDE | MAE | SDE | MAE | SDE |
| Linear Regression | 8.3 | 10.0 | 5.5 | 6.9 | 11.7 | 12.0 | 7.3 | 7.4 |
| Support Vectors | 6.7 | 10.2 | 5.2 | 7.0 | 10.2 | 11.1 | 6.5 | 7.3 |
| Random Forest | 5.9 | 11.4 | 4.1 | 7.5 | 8.9 | 10.2 | 5.7 | 5.9 |
| Adaptive Boosting | 5.7 | 8.9 | 3.7 | 7.1 | 7.6 | 9.2 | 4.8 | 5.1 |
| **Deep Neural Network** | **5.0** | **6.3** | **3.0** | **4.0** | **7.2** | **8.5** | **4.1** | **4.0** |

The bold face show values for Deep Neural network that we are utilizing in our algorithm.

Table II represents the results of our feature selection analysis for BP. We have scaled the scores of individual features for all four criteria between 0 and 1 for comparison purposes. Note that mRMR analysis returns the top 12 features and the remaining feature scores have been added from relevance analysis only i.e., PCC and MIC. As we can see, Spectral energies and statistical parameters like entropy and kurtosis are among the top features which are most relevant to the target BP values. Since the main variations in the FFT spectrum happen in bands 1 and 2, these bands prove to contain the most significant features after feature relevance and redundancy analysis.

### D. Estimation

After performing feature engineering, we use the most significant features for the estimation of RR and BP. Note that RR features i.e., RIIV, RIFV, and RIAV are checked for relative significance for every patient. However, the top 12 features of BP are the same for all patients, and feature engineering is not performed in the real system.

***1) RR Estimation:*** Based on the obtained good-quality modulation signals, RR is computed using a peak detector. A moving average filter with a frequency range of 0.1 to 1 Hz (6 to 60 bpm) is applied before estimating the respiration cycle period which simplifies the task of the peak detector. The average time between two peaks within a window is associated with one respiration cycle and it is reciprocally multiplied by 60 to find RR in bpm. Selected RR estimates from reliable modulations are then fused by finding the average to obtain one final RR value.

***2) BP Estimation:*** For BP estimation, different ML and deep learning algorithms have been used in the literature [34], [35]. We used simple linear regression, support vectors, ensemble learning methods (bagging, boosting), and deep learning methods for modeling the BP system. We have used Grid-Search with 10-fold cross-validation to find the best set of parameters. In addition, the data is not shuffled before training/testing, hence the data remains the same for all regression algorithms. Table III shows the performance comparison of these regression algorithms.

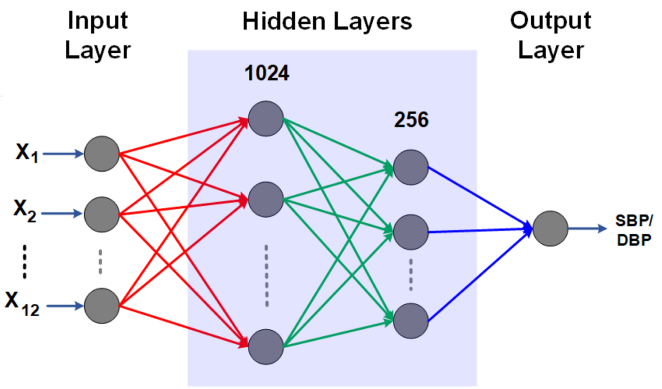


**Fig. 12.** Neural Network Architecture for BP estimation.

1) *Linear Regression:* The baseline ML algorithm for any data exhibiting a linear relation is linear regression. We selected the top 12 features from the PCC criteria. These models are easy to implement, less computational, and take less training time as compared to other ML methods. We used Scikit and NumPy libraries to train and cross-validate our algorithm by minimizing the residual sum of squares. We deployed 10-fold cross-validation to validate the generalizability of the model.
2) *Support Vector Regression:* Support Vector machines are kernel methods that use optimization to find the maximum margin between the support vectors. We did input the top 12 features from PCC selection method into the model. For choosing values of kernel transformation function and miss-penalty coefficient parameters, we used grid search with 5-fold cross-validation in Scikit-learn.
3) *Random Forest Regression (Bagging):* Random Forest is an ensemble learning method that deploys many decision trees in a parallel fashion. It averages the results of all trees trained on a subset of the dataset. We selected 12 most significant features according to the Mutual Information measure. The model was trained using grid search along with cross-validation to get optimal values of the number of trees.
4) *Adaptive Boost Regression (Boosting):* This is also an ensembling learning method that uses different estimators in a series fashion such that each new estimator learns from the mistakes of the previous estimator. Once again, we used decision trees as estimators and used mutual information as the feature selection criteria. Decision tree learning uses information gain as attribute selection criteria. That's why it is closely related to the information entropy of features.
5) *Deep Neural Network Regression:* We used deep learning as well where we built a neural network architecture as shown in Fig. 12. This model was finalized after trying different combinations of architecture parameters i.e., number of layers, number of hidden units in a layer, and activation functions. Similarly, the hyper-parameters of the neural network such as learning rate, batch size, and optimization algorithm i.e., Adam (adaptive moment estimation) parameters were selected. Note that we implemented the same Neutral Network (NN) architecture for both Systolic BP (SBP) and Diastolic BP (DBP. For the first hidden layer, we have:

$$Y_1 = W_1 * X + b_1, \tag{13}$$

$$A_1 = \tanh(Y_1), \tag{14}$$

Similarly, for second hidden layer:

$$Y_2 = W_2 * A_1 + b_2, \tag{15}$$

$$A_2 = \tanh(Y_2), \tag{16}$$

And finally, the output layer:

$$Y_3 = W_3 * A_2 + b_3, \tag{17}$$

## III. Results

### A. Datasets

We have used two open-source databases to validate our RR approach: The CapnoBase dataset (available at capnobase.org) and the BIDMC dataset derived from MIMIC-II database (available at https://mimic.physionet.org/), as described below:

1) *TBME Benchmark Capnobase Dataset:* This dataset has 8-minute recordings of 42 patients (29 pediatric and 13 adults). It consists of both controlled ventilation and spontaneous breathing cases. We adopted Capnometry waveform as the reference "gold standard" to validate the results. Both PPG and reference signals are sampled at 300 Hz.
2) *BIDMC Dataset from MIMIC-II Physionet:* This dataset contains 53 adult patient recordings, each 8 minutes in duration. We did a performance comparison using the reference thoracic impedance pneumography signal. The PPG and reference signals provided have been sampled at 125 Hz.

For BP validation, we used the Open-Source MIMIC-II database [36] which had 12000 subject recordings of different durations (accessed in November 2021). We performed dataset cleaning by selecting only those records having a minimum duration of 8 minutes to ensure enough recording period for reliable processing. This left us with approximately 2064 subjects. Then, we scanned the selected subjects for abnormal BP values (SBP$<$80, SBP$>$180, DBP$<$60, or DBP$>$130) using the given invasive ABP (arterial blood pressure) waveform which returned in 117715 windows of 8 seconds and 3167797 heartbeats, representing 1700 unique subjects in total. Both signals i.e., PPG and gold standard ABP have been sampled at 125 Hz which is sufficient to accurately extract temporal features from PPG [37].

Fig. 13 shows the distribution of BP values across the final selected records. We have divided the data into three BP levels according to ACC/AHA standards. The normal BP or Normotension corresponds to (90/60 - 130/80) mmHg in SBP/DBP while the abnormal levels are i) Hypotension: The low BP level is below 90/60 mmHg and ii) Hypertension: The high BP level

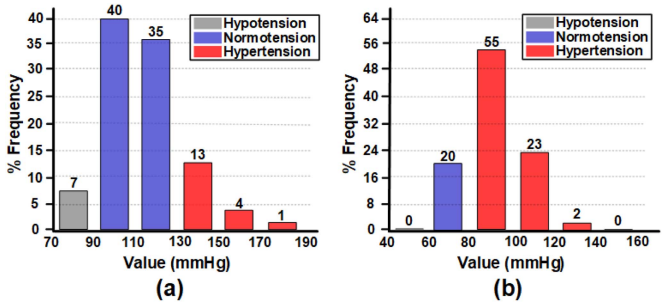


**Fig. 13.** Histograms showing Percentage number of values corresponding to a given BP level: (a) SBP and (b) DBP.

is above 130/80 mmHg. Similarly, Table VI gives some insight into database statistics having a wide range of BP values.

Since the previous studies have used the standard sampling rates provided with datasets, we have followed the same rule. This allows us to make performance comparisons with other state-of-the-art works. However, we will choose 125 Hz for both RR and BP in case of a hardware implementation of these methodologies because it would be sufficient to accurately extract temporal features from PPG for both RR and BP [37].

### B. Performance Evaluation

For RR, we adopted a 32-second moving window and shifted by 3 seconds to obtain the results. For the sake of comparison, a reference RR with the closest timestamp was adopted. We computed MAE in bpm for the entire moving windows for each patient. The patient-wise error distribution is presented in the form of a boxplot in Fig. 14(a) for the CapnoBase dataset and in Fig. 14(b) for the BIDMC dataset. Boxplots display the median and inter-quartile range (IQR) of MAE for individual modulations (RIIV, RIFV, and RIAV) without using any MQI, using each MQI separately (FFT, AC, XC-Tmp), and our proposed fusion approach using all MQIs i.e., MQI Fusion.

For BP, we used a window size of 8 seconds to evaluate the results. The reference values were generated using the given invasive ABP waveform. We measured mean absolute error (MAE) in mmHg for each patient over all windows. Table III represents a comparison of the performance of different ML algorithms. We implemented Linear Regression and kernel machines i.e., support vector regression. Then we used complex ensemble learning methods i.e., Random Forest and Adaptive Boost to increase the prediction power. Finally, the deep neural network performed best for BP estimation. We measured Pulse Pressure (PP) and Mean Arterial Pressure (MAP) as well.

For the selected DNN model, the regression plot, Bland-Altman Plot, and the patient-wise error distribution have been shown in Fig. 15 for both SBP and DBP. The regression plots show a strong correlation between actual and estimated BP values with high R and $R^2$ values. Similarly, the Bland-Altman plots show promising mean error and limits of agreement of error. In addition, the error histograms present a normal distribution of error. Since the MAE is $\leq$ 5 mmHg with a standard deviation $\leq$ 8 mmHg it meets the American Association for the Advancement of Medical Instrumentation (AAMI). Additionally, based on Fig. 15(e) and (f), the results also meet the British Hypertension Society (BHS) Class Criteria that require an absolute difference between standard and test device (%) is >60% for ($|$error$|$ $\leq$ 5 mmHg), >85% for ($|$error$|$ $\leq$ 10 mmHg), and >95% for ($|$error$|$ $\leq$ 15 mmHg) [38].

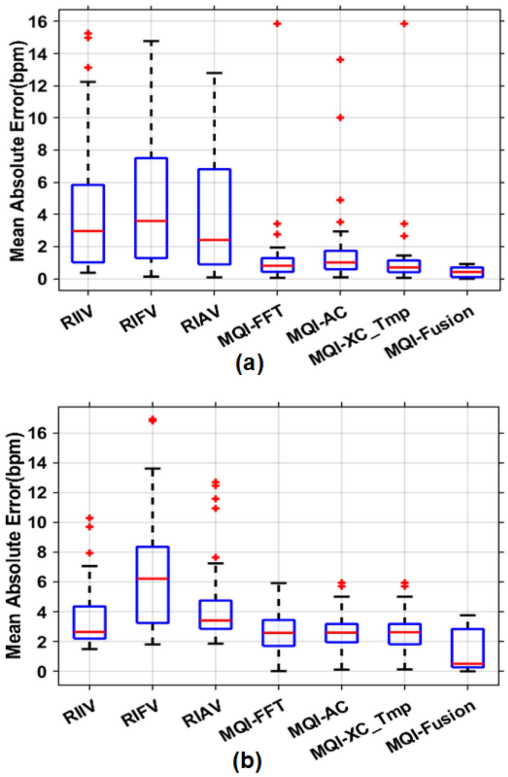


**Fig. 14.** Median and 25th to 75th percentiles of MAE for 32 seconds window size using individual modulations without a quality check (RIIV, RIFV, RIAV), using each quality measure one at a time (AC, FFT, XC-Tmp) and proposed fusion methodology using the entire quality measures (MQI-Fusion) for (a) CapnoBase and (b) BIDMC datasets.

### C. Performance Comparison

The proposed RR method offers superior performance compared to the current state-of-the-art with 3 robust respiration quality measures (RR quality measures), presented in Table IV. We obtained improved results on both datasets which means our proposed methodology performs equally well on a wide range of patients i.e. diverse patient cases. It involves both pediatric and adult patients in different clinical conditions. We utilized the entire PPG signal which means that the estimator is able to find at least one good-quality modulation for all the patients.

As presented in Table V, the proposed method for BP estimation offers robust results in terms of MAE and SDE. The state-of-the-art work [22], [39], [40] have used VG with transfer learning, CRNN, and adaptive regression, respectively, while we have used a simple 2-layer neural network. We have followed the "Data-Driven Approach" that enables us to have similar results

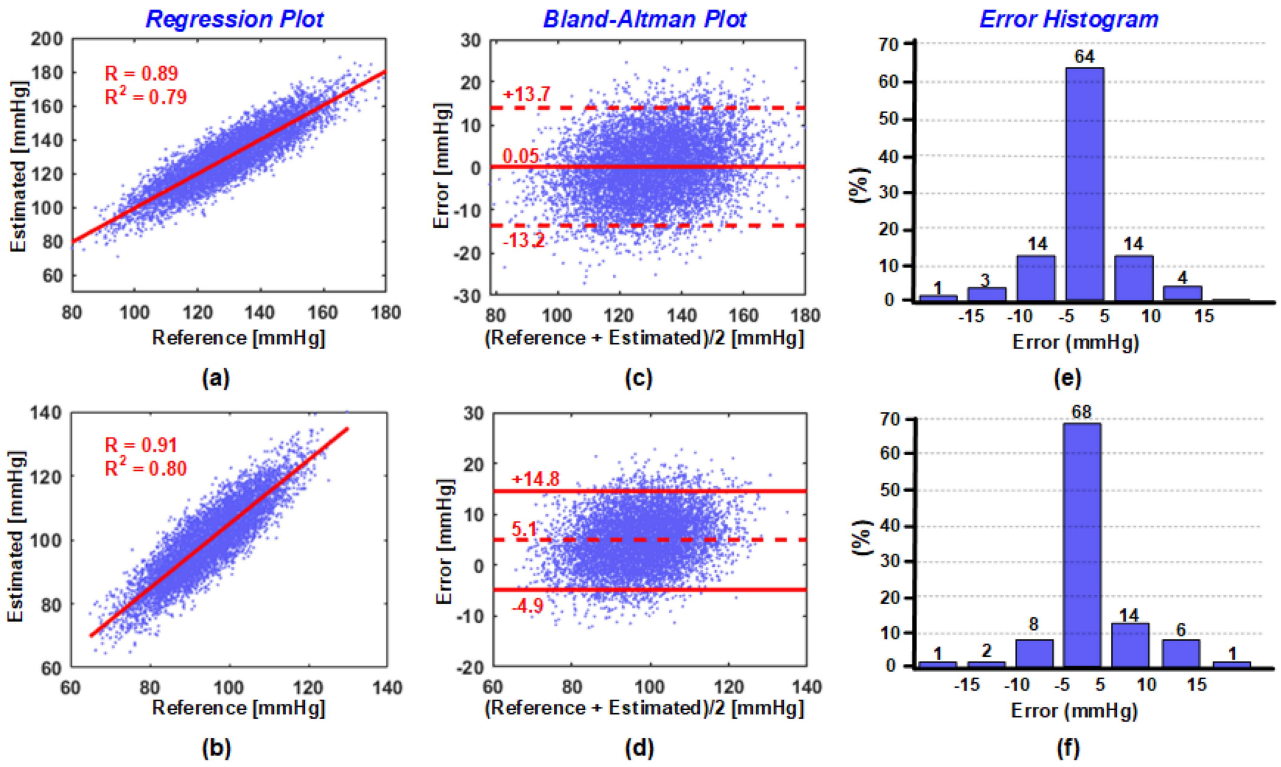


**Fig. 15.** Regression Plots for (a) SBP, and (b) DBP, Bland-Altman Plots for (c) SBP, and (d) DBP, and Error histograms for (e) SBP, and (f) DBP, where 'R' is the Pearson correlation coefficient and $R^2$ is the coefficient of determination. In Bland-Altman Plots, solid red lines indicate mean error while dotted red lines represent 95% confidence interval ($-1.96\sigma$ to $+1.96\sigma$) where '$\sigma$' stands for the standard deviation of error.

## TABLE IV

RR Comparison With State-of-The-Art (For 32 Sec Window Size With Both Datasets): Number of Patients Considered; Respiration Quality Analysis in Terms of Number of Quality Measures; MAE Presented as Median and Interquartile Range (25TH to 75TH Percentiles) and Percentage of Windows Discarded During Fusion

| Method | CapnoBase Dataset | | | | BIDMC Dataset | | | |
|---|---|---|---|---|---|---|---|---|
| | No. of Subjects | Resp. Quality Measures | RR MAE (bpm) | %windows discarded | No. of Subjects | Resp. Quality Measures | RR MAE (bpm) | %windows discarded |
| BSPC 2023 [15] | 42 | - | 0.37(0.19-1.42) | 0% | 53 | - | 0.89(0.36-3.05) | 0% |
| IoT J. 2023 [16] | 42 | - | 1.79 ±1.37 | - | 52 | - | 1.89 ±0.95 | - |
| EMBC 2021 [14] | - | - | - | - | 53 | 0 | 1.9 ±0.3 | - |
| ICAIoT 2022 [17] | - | 3 | 0.4(0.2-0.8) | 1.3% | 10 | 3 | 0.7(0.3-4.9) | 23.3% |
| TBME 2020 [19] | 42 | 3 | 0.5(0.2-1.1) | 0% | - | - | - | - |
| **Proposed** | **42** | **3** | **0.4(0.1-0.7)** | **0%** | **53** | **3** | **0.5(0.3-2.8)** | **0%** |

The bold face show the values for the proposed algorithms.

## TABLE V

BP Comparison With State-of-The-Art: Number of Patients Considered With Database; Number of Selected Features; Number of Physiological Signals Acquired; Used ML Model and Error in Terms of MAE and Standard Deviation Of Error (SDE) for Both SBP and DBP in UNITS of MMHG

| Method | No. of Subjects | No. of Selected Features | Channels Req. | Selected Regression Model | SBP MAE (SDE) in mmHg | DBP MAE (SDE) in mmHg |
|---|---|---|---|---|---|---|
| JBHI 2022 [27] | 348 (MIMIC DB) | data-driven | 1 (PPG) | Visibility Graph and Transfer Learning | 6.17(8.46) | 3.66 (5.36) |
| JBHI 2022 [28] | 100 (MIMIC DB) | - 100(Temporal) | 1 (only PPG) | CRNN | 3.52 (-) | 2.20 (-) |
| Sensors 2020 [26] | 942 (MIMIC DB) | - (only Physio) | 1 (only PPG) | AdaBoost Reg (200 DTs) | 8.2 (10.4) | 4.2 (4.2) |
| IEEE Sens. J. 2023 [22] | MIMIC | - | 2 (PPG + ECG) | U-Net model | PPG 17.51(20.98) ECG 19.10(21.42) | PPG 9.47(12.85) ECG 10.62(13.20) |
| Sensors 2021 [39] | 1131 (MIMIC DB) | - | 1 (only PPG) | Seq2seq + Attention | 14.39 (17.87) | 6.57 (8.43) |
| Sensors 2022 [40] | 435 | 10 (Physio + Demo) | 1 (only PPG) | Exponential Gaussian process Regression | - (15.6) | - (12.6) |
| JBHI 2021 [24] | 1376 (Vital DB) | 28 (only Physio) | 2 (PPG + ECG) | ANN + RNN | 5.1 (6.9) | 2.9 (4.0) |
| **Proposed** | **1690 (MIMIC DB)** | **12 (Physio + Spectral + Statistical)** | **1 (only PPG)** | **DNN (2 FC Layers)** | **5.0 (6.3)** | **3.0 (4.0)** |

The bold face show the values for the proposed algorithms.

with robust and a smaller number of features as compared to a larger number of features without feature engineering. We have deployed robust spectral and statistical features. Furthermore, we did feature optimization to select the most significant features only. Furthermore, we corroborated our research on a heterogeneous database having 1690 patient records. This provides clinical reliability for deploying BP monitors.

## IV. Discussion

We presented innovative respiration quality assessment measures to improve the fusion methodology by making it more robust for the average RR readings. The template matching cross-correlation MQI accurately identifies the respiratory modulations with high quality as shown in Figs. 9 and 10, respectively. The right-most box in Fig. 14 reflects an overall reduction in MAE when using the combined three MQIs to select the modulation for RR measurements. It has no outliers i.e., MQI Fusion performs well for all patients in both datasets. Similarly, histograms in Fig. 15 show that BP error is concentrated around 0 for both SBP and DBP. As shown in Table IV, the proposed method does not discard any PPG windows which means we always have RR readings, which is essential for continuous monitoring of vitals. The results show that the proposed method has better MAE performance compared to state-of-the-art works. The proposed approach is also independent of the patient's health condition, body position, or activity during measurement. Hence, users can have a wearable pulse oximeter sensor while performing normal daily activities.

As illustrated in Fig. 11, the performance of respiration quality measures changes with the value of the quality thresholds. If we assert strict threshold values, the MAE improves at the expense of discarding many PPG windows. However, we tune threshold values in such a way that we get desired performance while retaining all data windows in the final MQI fusion methodology. In addition, the empirical quality thresholds are not patient-specific, they are the same for the entire dataset which allows the proposed approach to be independent of individual patients.

The main challenge in developing a vitals monitoring device is the PPG morphology variation from patient to patient. PPG morphology changes as the measurement position, skin texture, and activity change. This is also dependent on individual person's cardiovascular characteristics. In this paper, we have implemented robust features which are independent of these factors and perform equally well on all patients. These features include physiological, spectral, and statistical parameters which we have proved to be highly correlated to the target variables. This results in improved performance compared to state-of-the-art methods as shown in Table V.

Another problem in adapting to the use of vital healthcare devices is the lack of reliability. Researchers so far have proposed a large number of methods for vitals estimation, but they have corroborated their approaches on small datasets having a little number of patients with less diversity of cases. The MIMIC-II database used is a heterogeneous standard database having a variety of cases in different clinical conditions (Fig. 15 and Table VI). We have validated our methodology on this extensive database to provide credibility for clinical use. In this way, we have added to the reliability of vital monitoring systems, having applications in mobile and fitness health-care devices.

**TABLE VI**
MIMIC DB Statistics of Selected Records Demonstrating the Range of BP Values

| | Min. | Max. | STD | Mean | Median |
|---|---|---|---|---|---|
| DBP (mmHg) | 65.1 | 129.7 | 12.7 | 91.1 | 89.3 |
| SBP (mmHg) | 80.0 | 180.0 | 20.1 | 114.3 | 111.7 |

For embedded applications, we must consider power efficiency. The main cost is the number of computations in terms of multiplications and additions of designed algorithms. The proposed methods in the literature are based on frequency-domain analysis which involves a lot of computations. Similarly, Machine Learning and Deep Learning approaches are computationally very intensive. They require specific hardware support as well. Therefore, we have selected the 12 most significant features only (Table II) by performing feature relevance analysis to reduce the computational load. Future work needs to emphasize on developing less computational, and more efficient algorithms to measure vital signs.

For continuous monitoring of vital signs, another important aspect is the Hardware Complexity involved. Current methods using two physiological sensors are not only computationally intensive but also the implemented devices are complex. They require two sensors for acquiring two signals i.e., PPG and ECG which might be from two different body positions. For continuous wear, these devices are not comfortable to carry. However, we have tried to minimize the subject's distress by using one pulse oximeter sensor for PPG only. This results in a simple wearable device that gives continuous estimates of RR and BP. Such a device is convenient to wear and carry for a long time use.

## V. Conclusion

In this paper, we alleviated the problem of patient dependency in the measurement of vital health signs. For diverse patients with variations in PPG physiology, we proposed a patient-independent approach using robust Spectro-Temporal features to increase the reliability of the BP estimation methodology. To tackle the variations in extracted physiological features for RR estimation, we introduced powerful feature selection measures. We have validated our research findings on a large database MIMIC having diverse patient cases in different clinical conditions. The obtained results prove the robustness of our approach and meet the required clinical standards. Our proposed approach requires only one physiological signal i.e., PPG to estimate both vitals i.e., RR and BP. By acquiring single-channel PPG using one convenient wearable sensor, we have enabled continuous monitoring of vital health signs in a non-invasive manner. Our research finds applications in fitness, remote, and mobile health-care devices such as smartwatches where one can monitor vital health signs continuously in a non-invasive way while performing daily life activities.

## REFERENCES


[1] Y. Guo et al., "A review of wearable and unobtrusive sensing technologies for chronic disease management," *Comput. Biol. Med.*, vol. 129, Feb. 2021, Art. no. 104163.

[2] S. L. Stevens et al., "Blood pressure variability and cardiovascular disease: Systematic review and meta-analysis," *Brit. Med. J. (Clinical Res.)*, vol. 354, Aug. 2016, Art. no. i4098.

[3] J. E. Fergeson et al., "Acute asthma, prognosis, and treatment," *J. Allergy Clin. Immunol.*, vol. 139, no. 2, pp. 438–447, 2017.

[4] A. Adami, R. Boostani, F. Marzbanrad, and P. H. Charlton, "A new framework to estimate breathing rate from electrocardiogram, photoplethysmogram, and blood pressure signals," *IEEE Access*, vol. 9, pp. 45832–45844, 2021.

[5] Y. Fang, Z. Jiang, and H. Wang, "A novel sleep respiratory rate detection method for obstructive sleep apnea based on characteristic moment waveform," *J. Healthc Eng.*, vol. 2018, pp. 1–10, Jan. 2018.

[6] O. Marrone and M. R. Bonsignore, "Blood-pressure variability in patients with obstructive sleep apnea: Current perspectives," in *Nat. Sci. Sleep*, vol. 10, pp. 229–242, Aug. 2018.

[7] M. A. Cretikos et al., "Respiratory rate: The neglected vital sign," in *Med. J. Australia*, vol. 188, no. 11, pp. 657–659, Jun. 2008.

[8] Y. Yeghiazarians et al., "Obstructive sleep apnea and cardiovascular disease: A scientific statement from the American Heart Association," *Circulation*, vol. 144, no. 3, pp. e56–e67, 2021.

[9] Z. B. Zhou et al., "Wearable continuous blood pressure monitoring devices based on pulse wave transit time and pulse arrival time: A review," *Materials (Basel)*, vol. 16, no. 6, Mar. 2023, Art. no. 2133.

[10] R. Narasimhan, T. Parlikar, G. Verghese, and M. V. McConnell, "Finger-wearable blood pressure monitor," in *Proc. IEEE Conf. Eng. Med. Biol. Soc.*, 2018, pp. 3792–3795.

[11] I. C. Jeong, D. Bychkov, and P. C. Searson, "Wearable devices for precision medicine and health state monitoring," *IEEE Trans. Biomed. Eng.*, vol. 66, no. 5, pp. 1242–1258, May 2019.

[12] V. G. Ganti, A. M. Carek, B. N. Nevius, J. A. Heller, M. Etemadi, and O. T. Inan, "Wearable cuff-less blood pressure estimation at home via pulse transit time," *IEEE J. Biomed. Health Informat.*, vol. 25, no. 6, pp. 1926–1937, Jun. 2021.

[13] P. H. Charlton et al., "Breathing rate estimation from the electrocardiogram and photoplethysmogram: A review," in *IEEE Rev. Biomed. Eng.*, vol. 11, pp. 2–20, 2018.

[14] S. A. H. Aqajari, R. Cao, A. H. A. Zargari, and A. M. Rahmani, "An end-to-end and accurate PPG-based respiratory rate estimation approach using cycle generative adversarial networks," in *Proc. IEEE Eng. Med. Biol. Soc.*, 2021, pp. 744–747.

[15] H. J. Davies and D. P. Mandic, "Rapid extraction of respiratory waveforms from photoplethysmography: A deep corr-encoder approach," *Biomed. Signal Process. Control*, vol. 85, pp. 1–8, Aug. 2023.

[16] P. Osathitporn et al., "RRWaveNet: A compact end-to-end multiscale residual CNN for robust PPG respiratory rate estimation," *IEEE Internet Things J.*, vol. 10, no. 18, pp. 15943–15952, Sep. 2023.

[17] G. N. K. Reddy, M. S. Manikandan, and R. B. Pachori, "Automated hilbert envelope based respiration rate measurement from PPG signal for wearable vital signs monitoring devices," in *Proc. IEEE Int. Conf. Artif. Intell. Things*, 2022, pp. 1–6.

[18] M. A. Sultan and W. Saadeh, "Robust estimation of respiratory rate from photoplethysmogram with respiration quality analysis," in *Proc. Conf. IEEE Int. Symp. Circuits Syst.*, 2022, pp. 65–69.

[19] S. Khreis, D. Ge, H. A. Rahman, and G. Carrault, "Breathing rate estimation using Kalman smoother with electrocardiogram and photoplethysmogram," *IEEE Trans. Biomed. Eng.*, vol. 67, no. 3, pp. 893–904, Mar. 2020.

[20] C.-Y. Guo, C.-C. Chang, K.-J. Wang, and T.-L. Hsieh, "Assessment of a calibration-free method of cuffless blood pressure measurement: A pilot study," *IEEE J. Transl. Eng. Health Med.*, vol. 11, pp. 318–329, 2023.

[21] Z.-D. Liu et al., "Cuffless blood pressure measurement using smartwatches: A large-scale validation study," *IEEE J. Biomed. Health Inform.*, vol. 27, no. 9, pp. 4216–4227, Sep. 2023.

[22] R. Yoshizawa, K. Yamamoto, and T. Ohtsuki, "Investigation of data leakage in deep-learning-based blood pressure estimation using photoplethysmogram/electrocardiogram," *IEEE Sensors J.*, vol. 23, no. 12, pp. 13311–13318, Jun. 2023.

[23] M. Sheeraz, A. R. Aslam, N. Hafeez, H. Heidari, and M. A. B. Altaf, "A wearable high blood pressure classification processor using photoplethysmogram signals through power spectral density features," in *Proc. IEEE 4th Int. Conf. Artif. Intell. Circuits Syst.*, 2022, pp. 198–201.

[24] S. Yang, J. Sohn, S. Lee, J. Lee, and H. C. Kim, "Estimation and validation of arterial blood pressure using photoplethysmogram morphology features in conjunction with pulse arrival time in large open databases," *IEEE J. Biomed. Health Inform.*, vol. 25, no. 4, pp. 1018–1030, Apr. 2021.

[25] F. Miao et al., "A novel continuous blood pressure estimation approach based on data mining techniques," *IEEE J. Biomed. Health Inform.*, vol. 21, no. 6, pp. 1730–1740, Nov. 2017.

[26] N. Hasanzadeh et al., "Blood pressure estimation using photoplethysmogram signal and its morphological features," *IEEE Sensors J.*, vol. 20, no. 8, pp. 4300–4310, Apr. 2020.

[27] W. Wang, P. Mohseni, K. L. Kilgore, and L. Najafizadeh, "Cuff-less blood pressure estimation from photoplethysmography via visibility graph and transfer learning," *IEEE J. Biomed. Health Inform.*, vol. 26, no. 5, pp. 2075–2085, May 2022.

[28] J. Leitner, P. -H. Chiang, and S. Dey, "Personalized blood pressure estimation using photoplethysmography: A transfer learning approach," *IEEE J. Biomed. Health Inform.*, vol. 23, no. 12, pp. 13311–13318, Jun. 2023.

[29] W. Wang, P. Mohseni, K. Kilgore, and L. Najafizadeh, "Cuff-less blood pressure estimation via small convolutional neural networks," in *Proc. Conf. IEEE Eng. Med. Biol. Soc.*, 2021, pp. 1031–1034.

[30] K. Selvakumar et al., "Realtime PPG based respiration rate estimation for remote health monitoring applications," *Biomed. Signal Process. Control*, vol. 77, Aug. 2022, Art. no. 103746.

[31] C. Orphanidou et al., "Signal-quality indices for the electrocardiogram and photoplethysmogram: Derivation and applications to wireless monitoring," *IEEE J. Biomed. Health Informat.*, vol. 19, no. 3, pp. 832–838, May 2015.

[32] E. Sabeti et al., "Signal quality measure for pulsatile physiological signals using morphological features: Applications in reliability measure for pulse oximetry," *Inform. Med. Unlocked Elsevier*, vol. 16, 2019, Art. no. 100222.

[33] Y. Wang, X. Li, and R. Ruiz, "Feature selection with maximal relevance and minimal supervised redundancy," *IEEE Trans. Cybern.*, vol. 53, no. 2, pp. 707–717, Feb. 2023.

[34] P. C. P. Chao, C. -C. Wu, D. H. Nguyen, B. -S. Nguyen, P. -C. Huang, and V. -H. Le, "The machine learnings leading the cuffless PPG blood pressure sensors into the next stage," *IEEE Sensors J.*, vol. 21, no. 11, pp. 12498–12510, Jun. 2021.

[35] A. Rehman, M. A. B. Altaf, and W. Saadeh, "A 73 $\mu$W single channel photoplethysmography-based blood pressure estimation processor," in *Proc. IEEE Int. Symp. Circuits Syst.*, 2022, pp. 2318–2322.

[36] M. Kachuee, M. M. Kiani, H. Mohammadzade, and M. Shabany, "Cuff-less high-accuracy calibration-free blood pressure estimation using pulse transit time," in *Proc. IEEE Conf. Int. Symp. Circuits Syst.*, 2015, pp. 1006–1009.

[37] A. Choi and H. Shin, "Photoplethysmography sampling frequency: Pilot assessment of how low can we go to analyze pulse rate variability with reliability?," *Physiol. Meas.*, vol. 38, no. 3, 2017, Art. no. 586.

[38] E. O'Brien et al., "Blood pressure measuring devices: Recommendations of the European Society of Hypertension," *BMJ.*, vol. 322, no. 7285, pp. 531–536, Mar. 2001.

[39] N. Aguirre et al., "Blood pressure morphology assessment from photoplethysmogram and demographic information using deep learning with attention mechanism," *Sensors (MDPI)*, vol. 21, no. 6, 2021, Art. no. 2167.

[40] J. W. Chen et al., "A data-driven model with feedback calibration embedded blood pressure estimator using reflective photoplethysmography," *Sensors (MDPI)*, vol. 22, no. 5, 2022, Art. no. 1873.